# Origin of the intense positive and moderate negative atmospheric electric field variations measured during and after Antarctic blizzards

Yasuhiro Minamoto, Masashi Kamogawa, Akira Kadokura, Satoshi Omiya,
Naohiko Hirasawa, Mitsuteru Sato

**Corresponding author**

Masashi Kamogawa
kamogawa@u-shizuoka-ken.ac.jp
Global Center for Asian and Regional Research, University of Shizuoka
3-6-1,Takajo, Aoi-Ku, Shizuoka-City, Shizuoka Prefecture, 420-0839, Japan

**Abstract**

There is an atmospheric electric field (AEF) or an electric potential gradient (PG) in fair weather between the Earth's surface and the mesosphere/ionosphere, which is positive. During blizzards/snowstorms in the polar regions, an intense positive AEF/PG in the order of $10^3$ V/m of the same polarity in fair weather was observed using an electric field mill at 1.4 m in height. In contrast, a moderately negative AEF/PG variation after a blizzard was observed in 2015 at Syowa Station, Antarctica. The negative variation, where the magnitude ranged from tens to hundreds of V/m, gradually recovered into the positive AEF/PG for more than 40 minutes. According to various studies on blowing/drifting snow dynamics and electricity in laboratory experiments and field observations, snow particles colliding with the snow surface are charged, and the charge of saltating and suspended particles during the snowstorm is negative on average. To verify the AEF/PG observed during and after the blizzards, we numerically estimated the electric field surrounding the conductive sensor unit of the electric field mill using a three-dimensional Poisson equation. Under blizzard conditions, the polarity of the estimated AEF/PG was the opposite of that of the observed AEF/PG. From the noise study of the field mill, we deduced that the positive AEF/PG variations were caused by the collision of negatively charged snow particles with the electric probe on the sensor unit. Just after the blizzard, the number of snow particles measured at 4.4 m in height clearly decreased, and the camera image showed clear visibility. From this evidence, we modeled the suspended and saltating negatively charged snow particles that had fallen onto the ground surface and then constructed a charge layer of the snow particles softly attaching to the ground, which slowly discharged following the study on the electrical resistance of the powders. The three-dimensional Poisson calculation based on the model reproduced a moderately negative AEF/PG. Thus, we elucidated that the origins of the intense positive and moderate negative electric fields during and after blizzards are the charged snow particles colliding with the electric probe on the sensor unit and the negative snow layers softly attached to the ground, respectively. These results

are applicable to studies on dust storm electrification on Mars' and Earth's deserts, snowstorm electrification in the polar regions, and high mountains, such as Mt. Fuji in Japan, and turbulent electrification for industrial dust, which provides the identification of intense electrification and storms.

**Keywords**

Atmospheric electric field; Potential gradient; Electric field mill; Blizzard; Antarctica; Charged snow particles.

## 1. Introduction

There is an atmospheric electric field (AEF) in fair weather between the Earth's surface and the mesosphere/ionosphere. The magnitude of the AEF at the ground surface is around 100 V/m in fair weather at sea level (MacGorman and Rust, 1998; Harrison, 2013; Williams and Mareev, 2014). The AEF transports atmospheric ions originating from atmospheric molecules ionized by cosmic rays and natural radionuclides as air-earth currents (i.e., a weak electric current flow from the mesosphere/ionosphere to the ground surface). Negative charges are transported from the negatively polarized bottom of clouds to Earth's surface via negative ground-to-ground lightning, which occurs constantly all over Earth. The positive charges in thunderclouds are transported into the mesosphere/ionosphere, generating an electric potential difference in relation to Earth. The negatively charged precipitation also transports negative charges to Earth's surface (Liu et al., 2010). This electrical circuit on Earth is called the global electrical circuit (MacGorman and Rust, 1998; Harrison, 2004; Williams and Mareev, 2014). The electric potential difference between Earth's surface and the mesosphere/ionosphere, which forms a massive global-scale spherical capacitor, is around 250 kV (Markson, 2007). The downward (geocentric direction) of the vertical AEF is conventionally defined as positive. In other words, it is a positive AEF under fair-weather conditions. This definition is adopted in many studies of atmospheric electricity and many papers.

With the electric field vector and the electric potential expressed as $\boldsymbol{E}$ and $V$, respectively, $\boldsymbol{E}$ is given as follows:

$$\boldsymbol{E} = -\nabla V. \qquad (1)$$

When only the vertical $z$-axis is discussed, as in the case of the AEF in fair weather, equation (1) is expressed as follows:

$$E_z = -\frac{dV}{dz}. \qquad (2)$$

Here, we introduce the electric potential gradient (PG), which is a scalar quantity:

$$\mathrm{PG} = E_z. \qquad (3)$$

In this case, PG and $E_z$ have the same magnitude. Therefore, PG has also been used in some papers as a general expression because it is positive, like the AEF in fair weather (e.g., Harisson, 2013; Aplin, 2018; Nicoll et al., 2019). The present paper follows this definition for AEF/PG unless otherwise noted.

According to the World Meteorological Organization (1966), blowing snow was defined as snow raised by the wind to moderate heights above the ground, reducing horizontal visibility at eye level. The same source defined a snowstorm as a meteorological disturbance giving rise to a heavy fall of snow, often accompanied by strong winds, and a blizzard as a violent winter storm lasting at least 3 hours. It is combined with below-freezing temperatures and extremely strong wind laden with blowing snow, which reduces visibility to less than 1 km. Blizzards at Syowa Station, Antarctica (69°00'S, 39°35'E) have been identified by the criteria described in Sato and Hirasawa (2007), including visibility of less than 1 km and wind velocity of more than 10 m/s continuing for more than 6 hours. The blizzard at Syowa Station is regarded as a weather event as defined by these criteria.

In blowing snow conditions, including snowstorms and blizzards, an intense positive AEF/PG accompanied by high-frequency fluctuations was observed using an electric field mill. Gordon and Tylor (2009) measured the AEF/PG for 80 days in Amundsen Bay, Canada (70°03'N, 126°18'W) and observed intense positive variations of the AEF/PG during blowing snow events. In a polar observation, Kikuchi (1970) reported an intense positive AEF/PG observed during a blizzard at Syowa Station. Although the wind velocity and magnitude of the AEF/PG were correlated in previous studies (e.g., Kikuchi, 1970; Gordon and Tylor, 2009), the origin of the positive AEF/PG was unclear.

The dynamics of blowing snow involve the dynamics of snow drifting near the snow surface. During snow drifting, the dynamics of snow particles produces an electrical charge, categorized into the following three modes: saltation, suspension, and surface creep (Nemoto and Nishimura, 2004). Saltation refers to snow bouncing at the snow surface and/or pushing one particle out of another; suspension refers to snow migrating without touching the ground surface; and creeping refers to snow migrating, frequently in contact with the snow surface. When a snowstorm begins, the snow particles on the snow surface migrate as the wind speed increases, causing creep. The creep of the particles develops into saltation, which generates suspension (Anderson, 1987; Nemoto and Nishimura, 2004). When the snowstorm terminates, the suspended and saltating particles diminish.

Snow particles that collide with the snow surface are charged. Maeno et al. (1985) executed a laboratory experiment to collide positively and negatively charged snow seeds with snow surfaces under horizontal wind blowing inside a horizontal wind tunnel. The blowing snow particles were negatively charged, regardless of the initial seed polarity. The charge-to-mass ratio of the snow particles after the collision was −0.1 to −0.3 μC/kg. As described below, the amount of negative charge measured in the laboratory experiment was two orders of magnitude smaller than that observed in the field. Omiya and Sato (2011) examined the correlation between the electric charge of snow particles and their saltation in the same type of laboratory experiment as Maeno et al. (1985). They showed that the negative charge of snow particles accumulated with an increase in saltation occurrences. This means that the saltation in the laboratory experiments was smaller than that in the field because of the limited length of the wind tunnel.

In 1967 and 1968, Wishart (1968) measured the amount of charge on snow particles during the snowstorms at Byrd Station, Antarctica (80°00'S, 119°30'W), using a Faraday cage and a charge electrometer. He conducted two observation campaigns for different height measurements. The first observation showed that the charge-to-mass ratio of snow particles ranged from −1.4 to −7.7 μC/kg at a wind velocity of 4.5 to 6.5 m/s in an air temperature of −5 to −6°C and a height of 50 cm; this corresponded to a wind velocity of 6.5 to 9 m/s at a height of 10 m. The second The second observation showed that the charge-to-mass ratio comprised roughly negative constant values, −0.05 μC/kg at a wind velocity of 4.5–6.5 m/s, air temperature of −9 to −12°C (snow temperature of −10 to −13 C), and height of 15 cm, corresponding to a wind velocity of 7.5–9 m/s and a height of 10 m. Schmidt et al. (1999) measured the charge amount of 11 individual drifting snow particles at Chimney Park, Wyoming, USA, and measured both positive and negative charges. The charge-to-mass ratios of six negatively charged snow particles and five positively charged snow particles ranged from −12 to −208 μC/kg and 1 to 72 μC/kg, respectively. Burrows and Hobbs (1970) measured the charge of 3,654 snow particles passing through an induction coil during a light snowfall at an altitude of 2,025 m on Mt. Olympic, Washington, USA, and showed that the proportions of positively and negatively charged snow particles were 52% and 48%, respectively. The charge amounts per snow particle were on the order of $10^{-14}$ to $10^{-12}$ C. In Sapporo, Japan, Asuma et al. (1988) measured the electric charge of individual precipitation particles on the ground and at altitudes of 100 m and 200 m using a moored balloon at a wind speed of less than 6 m/s. They showed that positively and negatively charged precipitation particles were dominantly found in the sky and near the ground surface, respectively. The charge amounts per snow particle were in the order of $10^{-13}$ to $10^{-12}$ C. Therefore, both the positively and negatively charged snow particles were measured for suspended snow particles in the field observations. However, the dominant charge was statistically negative for the particles that were saltating and suspended during snowstorms in field observations (Wishart, 1968; Latham and Montagne, 1970; Schmidt et al., 1999).

The studies described above have shown that although snow particles in wind tunnel experiments controlled for saltation were negatively charged, both positively and negatively charged particles were observed in the snow particles where saltation could not be confirmed in the field. The charge-to-mass ratios of the particles observed in the field observations were two orders of magnitude larger than those measured in the laboratory experiments. These results suggest that collisions between the snow particles and the snow surface should generate a larger negative charge accumulation on the particles; they imply that the difference in charge-to-mass ratios between field and laboratory experiments was caused by the difference in the number of collisions owing to the different lengths of saltation.

Negative (upward) AEF/PG has been observed on the ground when the polarity of the dominant charge above the field mill is negative, such as in thunderstorm events (e.g., Suzuki et al., 2011). Similary, multiple negatively charged snow particles during the snowstorm were suspended around the sensor unit of the electric field mill that measured AEF/PG. Therefore, one may surmise that the electric field direction was from the electrical probe of the sensor unit to the negatively charged snow particles. In this case, the measured value was negative, as was the case just below the thundercloud. It is not clearly understood why positive AEF/PGs were measured during the blizzard/snowstorm.

An intense positive AEF/PG exceeding 10 kV/m was reported at Syowa Station during blizzards (Kikuchi, 1970). In addition, as described below, a moderate negative AEF/PG of −30 to −110 V/m was observed with a duration of 50 to 100 minutes, just after the blizzard on several occasions. In this study, we show the time series of the AEF/PG, the wind velocity, and the number of snow particles during the intense positive AEF/PG in the blizzard, as well as the moderate negative AEF/PG just after the blizzard. Furthermore, we demonstrated the numerical calculation of the AEF/PG formed by the distribution of the negatively charged snow particles to investigate the origin of the positive and negative AEF/PG variations during and after the blizzard, respectively. We discuss how to construct the intense positive AEF/PG during the blizzard and the moderate negative AEF/PG just after the blizzard.

## 2. Observation

In this study, we used the data of the AEF/PG, the wind velocity, the number of precipitation particles (NPP), and still images recorded by a live camera at Syowa Station in 2015. Syowa Station is located on East Ongul Island, about 4 km east of Antarctica. Fig. 1 shows the location of Syowa Station and the observation points in the station. The electric field mill measures the magnitude and polarity of the AEF/PG estimated from the amount of electric charge on the electrical probes (stators), which are alternately shielded and exposed by a grounded rotor (MacGorman and Rust, 1998). We used a Boltek EFM-100 electric field mill to observe the AEF/PG. The time resolution of the measurement was 2 Hz; the median value of 120 measured values was taken as 1-minute representative values for the analysis. The sensor unit was installed at a height of 1.4 m, and the electric probe of the sensor unit faced not the zenith but the ground (an inverted sensor) to avoid noise originating from snow precipitation and rainfall.

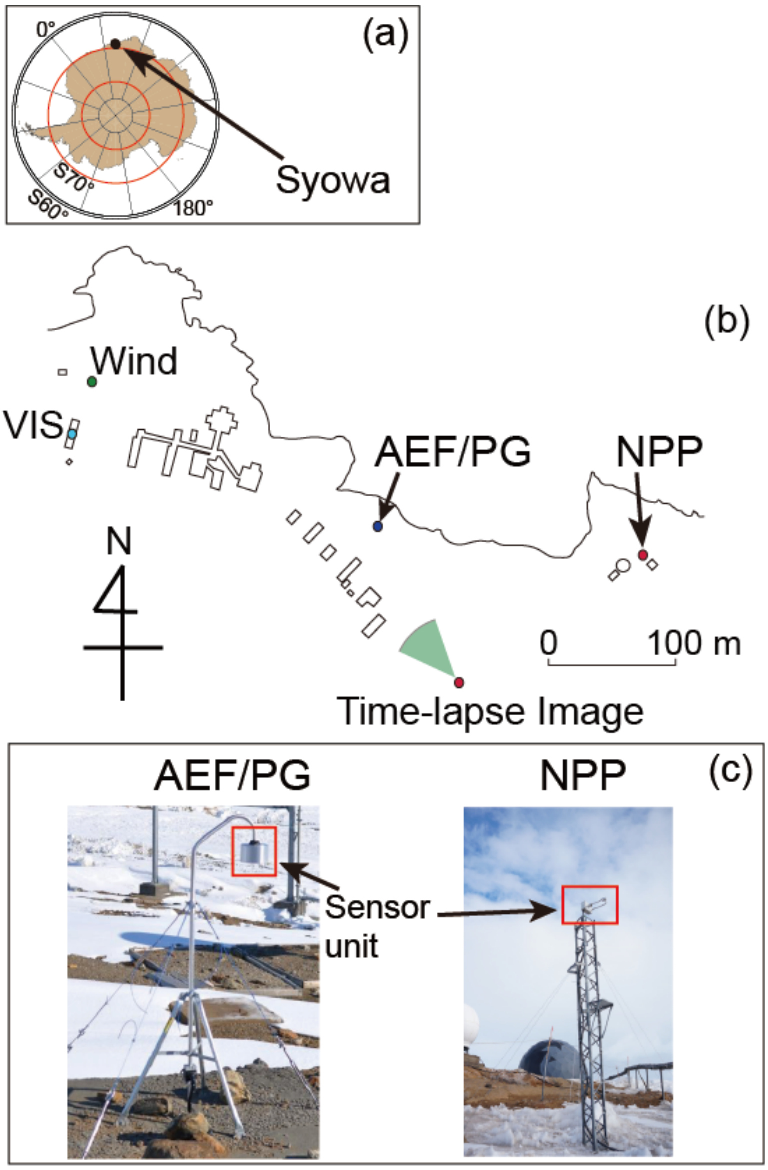


Fig. 1. (a) Location of Syowa Station, Antarctica, (b) observation points in the station, and (c) sensor photos of the atmospheric electric field (AEF)/potential gradient (PG) and the number of precipitation particles (NPP). The AEF/PG and NPP in (b) denote the location of the electric field mill to observe the AEF/PG and the laser precipitation monitor (LPM) sensor to observe the number and size of precipitation particles, respectively. The time-lapse image and the wind indicate the live camera and the location of the wind velocity sensor, respectively. Visibility (VIS) denotes the observation point for visibility.

The AEF/PG measured by an electric field mill does not correspond to the ambient AEF/PG in fair weather because the electric lines of force are concentrated around the conductive field-mill sensor, causing the intense AEF/PG. In addition, the electric conductive environment around the sensor also modulates the AEF/PG around the sensor. Hence, in general, the calibration is conducted, comparing the field mill for the observation and the field mill embedded in the ground (See Tsurudome et. al, 2013). Note that this calibration is effective for fair-weather observation and thunderstorms with a high cloud bottom. The calibration factor of the field mill for the present study (0.20) was obtained by the comparative observations described in MacGorman and Rust (1998). The measurement range of the present field mill was ±20 kV/m. Therefore, the observed range of AEF/PG was ±4,000 V/m, which is ±20 kV/m multiplied by the calibration factor.

The wind velocity data were 1-minute data provided by the Japan Meteorological Agency. The NPP, by size, was measured using a laser precipitation monitor (LPM). The sensor was installed at a height of 4.4 m. When the particles fell through the laser sheet between the laser emission part and the intensity detector, the size of the laser shadow behind the particles one by one was measured (Hirasawa et al., 2018). In this study, we used the 1-minute data of the number of particles and assessed the number of particles in the different classes measured as a distribution of snow particles before, during, and after the blizzard. The diameter of the precipitation particles was recorded as 22 diameter classes (i.e., 22 bins) by the LPM. However, we recategorized the particle diameter into the following four classes, because the major diameter of the precipitation particles was less than 0.500 mm: 0.125 mm or less, 0.250 mm or less, 0.375 mm or less, and more than 0.375 mm.

Regular observations of visibility were carried out eight times a day (i.e., every 3 hours). When there was an abrupt change in the weather, such as before and after the blizzard, a temporary observation was also conducted. To confirm the blizzard, we used time-lapse images provided by the live camera recording every 5 minutes (Figs. 5 and 7), which was installed 140 m away from the AEF/PG observation point (Fig. 1). The visibility to identify the blizzard was ocularly observed 500 m away from the live camera. In addition, visibility was not measured in a specified direction but in the direction with the most visibility. Therefore, the view direction of the live camera did not always coincide with that of the visibility observation. This may have caused differences in the timing of the start/end of the blizzard between the ocularly assessed visibility and the still images recorded by the live camera.

Fig. 2 shows the time series of the AEF/PG variations observed at Syowa Station from January to December 2015. Positive AEF/PGs were frequently observed, whereas negative electric fields were only occasionally seen. A positive AEF value exceeding 1 kV/m often lasted for several hours, whereas a negative value rarely lasted for more than 1 hour. Fig. 3 shows the relationship between the wind velocity and the AEF/PG from January to December 2015. As the wind velocity increased, the AEF/PG value and its variability increased. Indeed, below a wind velocity of 6 m/s, the AEF/PG value and its variability were smaller than those of the large wind velocity. Minamoto and Kadokura (2011) employed a threshold of 6 m/s for the criteria to identify fair-weather conditions. We note that when the wind velocity exceeded 26 m/s, the values of the 75th and 90th percentiles of the observed values were almost equivalent because of the saturation of the measurement.

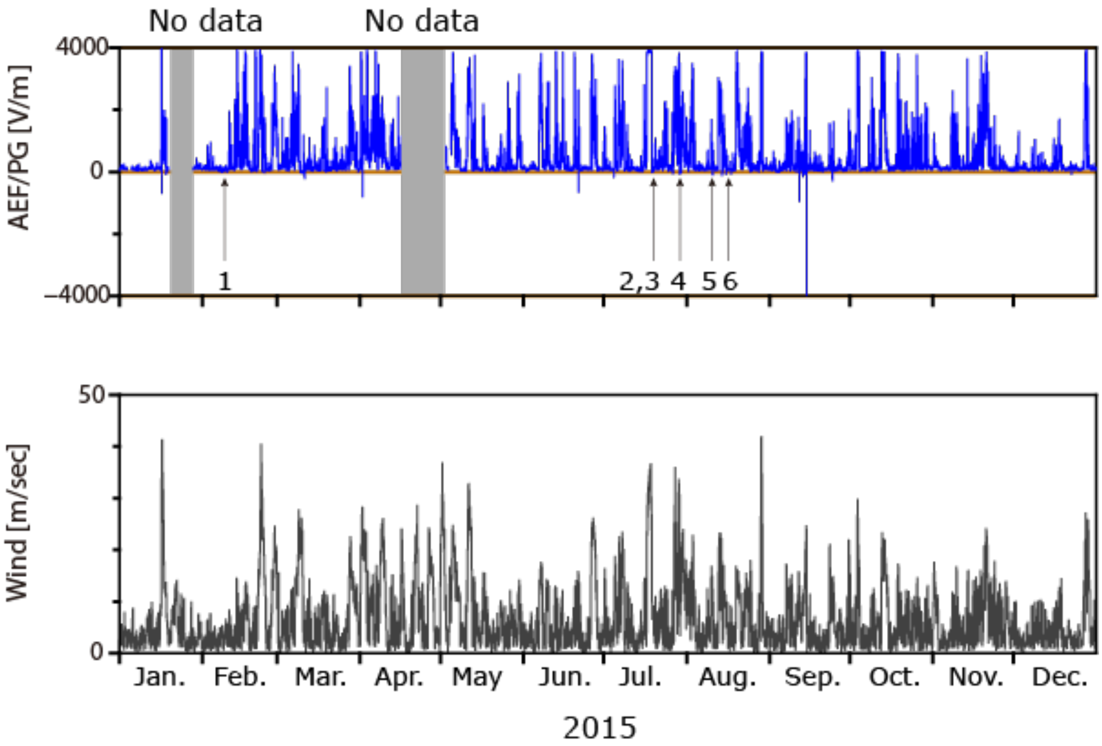


Fig. 2. Time series of 1-minute data of the AEF/PG and wind velocity in 2015 at Syowa Station. There are two data gaps, which are in January and from the middle of April to the beginning of May. The numbers below the AEF/PG panel correspond to the events of negative AEF/PG variations after the blizzard, as listed in Table 1.

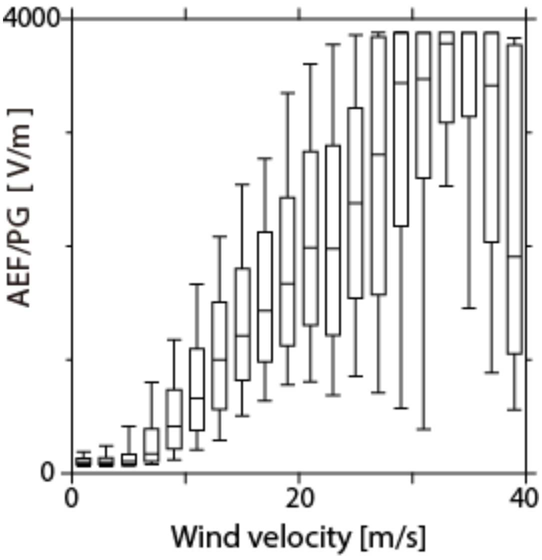


Fig. 3. Box-and-whisker plot for the relationship between wind velocity and the AEF/PG from January to December 2015. The whiskers and downside/middle/upside of the box indicate 10th, 25th, 50th, 75th, and 90th percentile values from the bottom. The class width of the wind velocity

was 2 m/s. The upper limit corresponding to a saturated value of the AEF/PG measurement was +4,000 V/m.

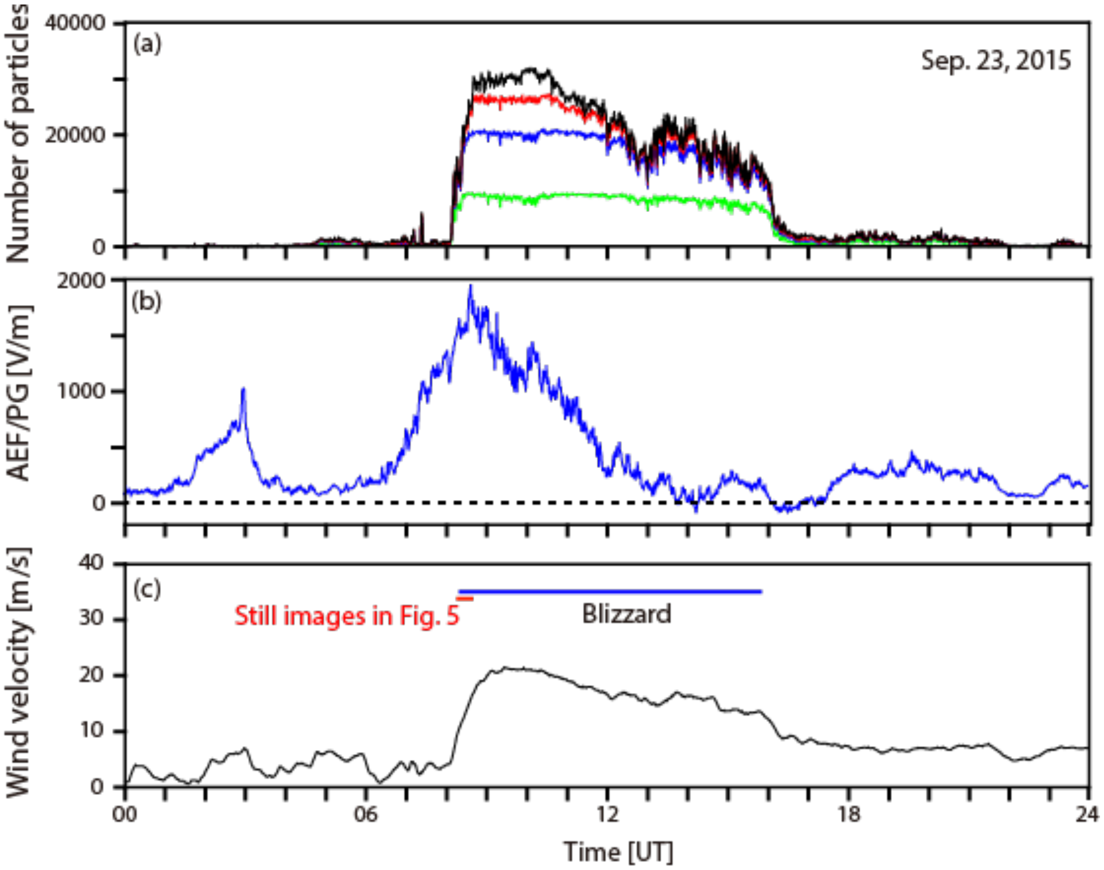


Fig. 4. Number of particles, AEF/PG, and wind velocity of 0 UT to 24 UT on September 23, 2015. (a) Number of particles in different particle size classes. The green, blue, red, and black lines indicate the number of particles with a diameter of 0.125 mm or less, 0.25 mm or less, and 0.375 mm or less, as well as the total number of particles. (b) AEF/PG. (c) Wind velocity. The blue and red bars denote the period of the blizzard and still images shown in Fig. 5, respectively.

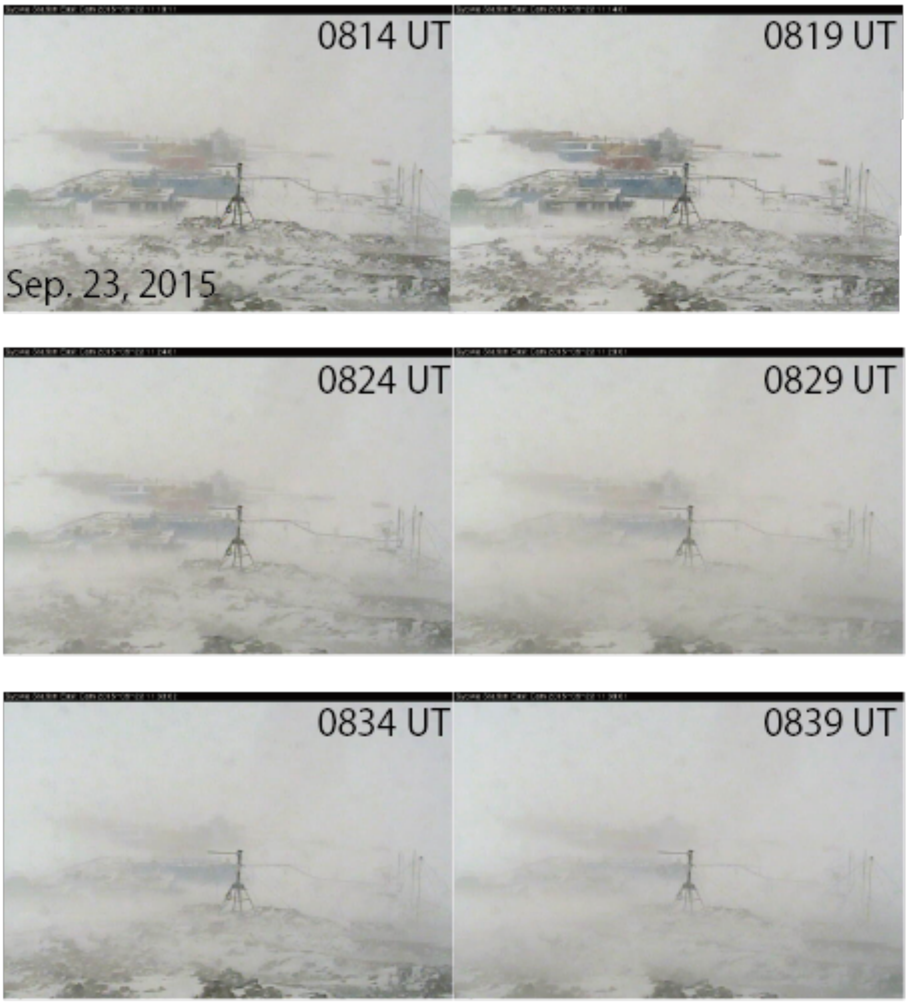


Fig. 5. Still images recorded every 5 minutes by the live camera from 0814 UT to 0839 UT on September 23, 2015.

Fig. 4 shows the time series of the number and size of snow particles, AEF/PG, and wind velocity on September 23, 2015, as an example of a blizzard period. The start and end of the blizzard were recorded at 0818 UT and 1550 UT, respectively (Oshiki, 2016). The wind velocity exceeded 6 m/s at 0810 UT and reached 20 m/s at 0900 UT. The AEF/PG and the number of particles increased rapidly around 0630 UT and 0700 UT, respectively. Note that we did not describe the origin of the enhancement of AEF/PG around 0300 UT not related to the increase in the number of snow particles and the wind. The origin was unknown, and similar variations were barely observed. Fig. 5 shows the still image of the live camera recording every 5 minutes from 0814 UT to 0839 UT on September 23, 2015. The visibility dropped between 0819 UT and 0824 UT. When the blizzard started at 0818 UT, the wind velocity was 16.5 m/s. Figs. 4 and 5 indicate that the number of particles measured by the LPM increased and the visibility decreased as the wind velocity increased.

Table 1. Six events of moderately negative AEF/PG variation after a blizzard in 2015. They were

satisfied with the conditions that the number of particles measured by the LPM was less than 500 and a negative AEF/PG was observed for more than 30 minutes. The start and end times of the negative AEF/PG after the blizzard are shown in the table. The minimum of the AEF/PG indicates the minimum value of the 5-minute running mean of the AEF/PG. The time constant $\tau$ is the period from the observed to the minimum value of the 5-minute running mean of the AEF/PG, $|E_{min}|$, to the value of $|E_{min}|/e$. The temperature refers to the hourly value observed during the negative AEF/PG.

| | Date (2015) | Start time (UT) | End time (UT) | Duration [min.] | Min. of AEF/PG [V/m] | Time constant $\tau$ [minutes] | Lowest wind velocity [m/s] | Highest wind velocity [m/s] | Temperature [°C] |
|---|---|---|---|---|---|---|---|---|---|
| 1 | Feb. 8 | 3:57 | 4:48 | 52 | −32.9 | 17 | 2.9 | 4.3 | −3.8 (04UT) |
| 2 | Jul. 19 | 2:41 | 3:42 | 62 | −39.4 | 36 | 5.9 | 7.1 | −11.5 (03UT) |
| 3 | Jul. 19 | 4:39 | 5:24 | 46 | −29.8 | 6 | 7.3 | 7.3 | −12.0 (05UT) |
| 4 | Jul. 29 | 10:06 | 11:44 | 99 | −101.2 | 58 | 3.8 | 8.2 | −6.8 (14UT) |
| 5 | Aug. 10 | 16:06 | 17:21 | 76 | −110.8 | 30 | 5.6 | 11.2 | −15.7 (17UT) |
| 6 | Aug. 15 | 14:42 | 15:33 | 52 | −63.1 | 14 | 5.3 | 8.9 | −13.7 (15UT) |

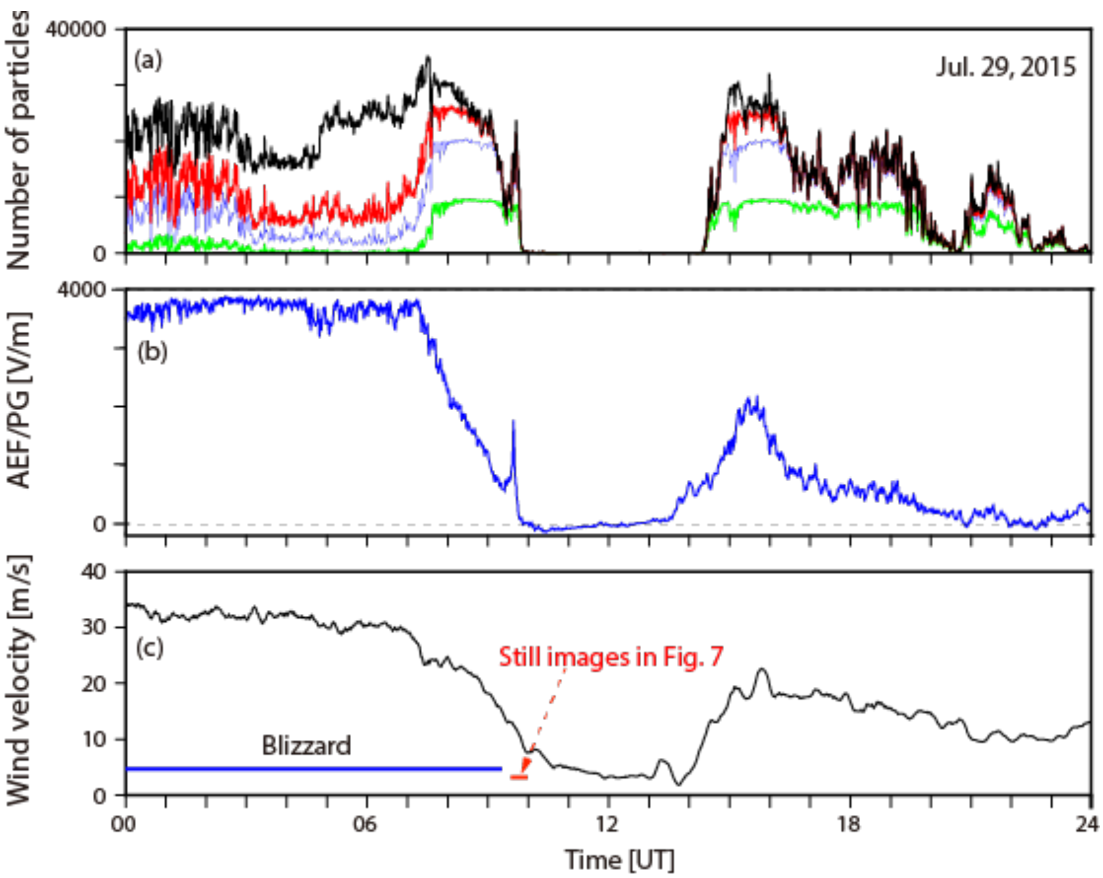


Fig. 6. Number of particles in different classes, AEF/PG, and wind velocity from 0000 UT to 2400 on July 29, 2015. The color of the lines is the same as in Fig. 4. The blue and red bars denote the period of the blizzard and still images shown in Fig. 7, respectively.


Fig. 7. Still images recorded every 5 minutes by the live camera from 0934 UT to 0959 UT on July 29, 2015.

Fig. 6 shows the time series of particle size distribution, AEF/PG values, and wind velocity from 0000 UT to 2400 UT on July 29, 2015. The blizzard ended at 0920 UT (Oshiki, 2016). The negative AEF/PG started at 0952 UT, and the negative values remained from 1001 UT to 1238 UT. Meanwhile, the NPP measured by the LPM at a height of 4.4 m was under 500. The recovery of visibility was recognized from the still images shown in Fig. 7. The AEF/PG values reached a minimum just after the blizzard ended and gradually recovered. The high-frequency fluctuation was not found in the recovery period.

Thirty blizzards were identified at Syowa Station in 2015 (Yamamoto et al., 2015; Oshiki, 2016). Among them, six events of similar negative variations in AEF/PG were found, as shown in Fig. 2. Table 1 lists the six events in 2015 that satisfied the conditions in which the negative AEF/PG values remained for more than 30 minutes and the number of particles measured by the

LPM was less than 500. The date, start/end time, duration, minimum AEF/PG, time constant, lowest/highest wind velocity, and temperature for each event are also shown. The time constant τ for the recovery of the negative AEF/PG was estimated from the period of the observed minimum value of the 5-minute running mean of the AEF/PG, $|E_{min}|$, to the value of $|E_{min}|/e$, where $e$ is the base of the natural logarithm. Although there was no significant correlation between the lowest/highest wind velocities or temperatures and the time constant τ, correlations between the minimum AEF/PG $|E_{min}|$ and time constant τ were obtained. Fig. 8 illustrates the semi-logarithmic relationship of the time constant τ and the minimum of the 5-minute running mean of the AEF/PG $|E_{min}|$. From these six events, the correlation coefficient between the time constant τ and the log $|E_{min}|$ of the minimum AEF/PG was 0.65.

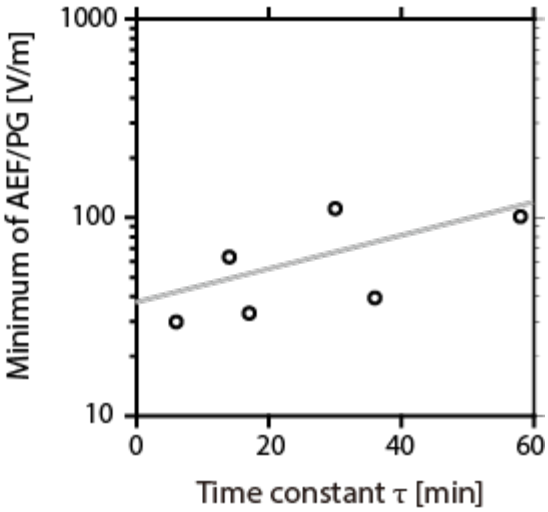


Fig. 8. Relationship between the minimum value of the 5-minute running mean of the AEF/PG and the time constant $\tau$ in the six events satisfied the conditions that the number of particles measured by the LPM be less than 500 and a negative electric field was observed for more than 30 minutes, as listed in Table 1. The horizontal axis is the time constant τ, the period from the observed minimum value of the 5-minute running mean of the AEF/PG, $|E_{min}|$, to the value of $|E_{min}|/e$. The minimum value of the 5-minute running mean of the AEF/PG is logarithmically shown on the vertical axis. The gray line is a regression line. The correlation coefficient between the time constant $\tau$ and the log $|E_{min}|$ is 0.65.

## 3. Calculations

Several previous papers have numerically investigated the electric field distribution formed by charged particles, such as snow and sand particles. Schmidt and Dent (1993) estimated the electric field intensity perpendicular to the surface when charged snow particles were arranged in a hexagonal configuration on the surface. They obtained an electric field of 1,000 V/m and 20 V/m at heights of 1–2 cm and 10 cm, not considering the charge of the snow particles suspended in the air. Gordon and Tylor (2009) proposed a model of the electric field formed by suspended snow particles. They found that the electric field intensity was proportional to the particle number density distribution in the model. However, the correlation coefficient $r$ between the electric field intensity and the snow-particle density in the field was relatively small, at $r^2 = 0.13$ to $r^2 = 0.66$. The researchers concluded that the intensity of the electric field was likely influenced by various other origins, such as snow conditions, the distribution of blowing snow density, and the history of suspended particles. Zheng et al. (2004) constructed a theoretical model for calculating the electric fields produced by charged sand particles, considering the saltation, suspension, and creep of the particles. The result of the calculation, in which the charge-to-mass ratio of sand particles was −60 $\mu$C/kg, similar to the charge-to-mass ratio of snow particles, showed that an upward electric field (i.e., a negative AEF/PG), exceeding 100 kV/m, was obtained just above the surface of the sand layers. The electric field decreased quickly to zero, while the height increased. Then, the polarity of the electric field changed (i.e., positive [downward]).

To verify the electric field distribution formed by the negatively charged snow particles suspended in the snowstorm, we numerically solved the three-dimensional Poisson equation. This is shown in equation (4):

$$\frac{\partial^2 \varphi\,(x,y,z)}{\partial z^2} = -\frac{\rho(x,y,z)}{\varepsilon_0} = -\frac{dE(x,y,z)}{dz}, \qquad (4)$$

where $\varphi(x, y, z)$, $\rho(x, y, z)$, and $E(x, y, z)$ are the electric potential, charge density, and electric field, respectively; $x$ and $y$ are the horizontal components; and $z$ is the vertical height from the ground.

Although a downward (geocentric) direction is conventionally defined as positive in the studies of atmospheric electricity, as introduced in Section 1, we define the upward direction as positive in this numerical calculation. In this section, not AEF/PG but the electric field is used to describe the calculated electric field in the Poisson equation because the horizontal components are also required to calculate the electric field around the sensor.

The computational domain of 6 m in the horizontal direction ($x$ and $y$ components) and 2 m in the vertical direction ($z$-component) was set. Although the prevailing wind direction was set in the $y$-axis (Fig. 9), the charge distribution $\rho(x, y, z)$ was regarded as uniform in the horizontal $x$ and $y$ components because the constant wind velocity substantially carried the constantly charged snow particles. In addition, the wind velocity concerned was much smaller than the electric field propagation velocity (i.e., the velocity of light); the charge distribution was practically time-independent (i.e., static). It must be noted that the electrical conductivity modification caused by the snow particles was negligible; Shumilov et al. (2005) showed that no significant change in atmospheric conductivity during the snowstorm was found at sites of high latitude in Russia. In the calculations, the electric field mill and its metal mounting support (Fig. 1) are conductors and are grounded, setting their potential to be zero and forming the boundary conditions shown in Fig. 9. To reproduce the AEF/PG in fair weather (i.e., 100 V/m in the geocentric direction), a positive charge layer was installed at the top of the computational domain as a boundary condition.

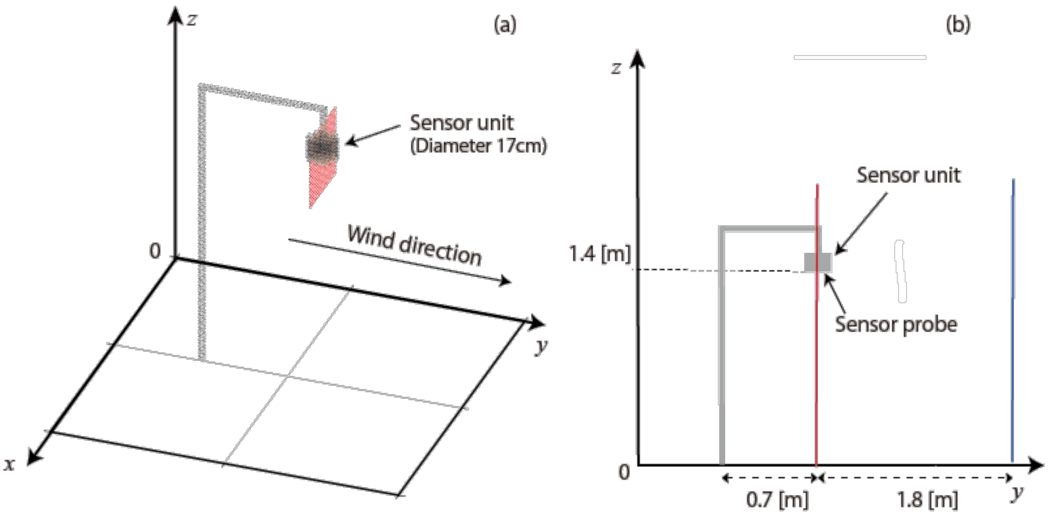


Fig. 9. Conductor for the boundary condition (i.e., the sensor unit of the electric field mill and the pipe for mounting the sensor) shown in the Poisson calculation. The sensor was mounted at a height of 1.4 m. The cross-sections of the Poisson calculation results (shown in Figs. 11 and 13) correspond to the red plane in (a). The vertical component *z* of the Poisson calculation results (shown in Figs. 12 and 14) corresponds to the red and blue lines in (b). The computational domain is 6 m in the horizontal *x*- and *y*-directions and 2 m on the vertical *z*-axis.

The negative charge density originating from the snow particles was given as an initial condition, multiplying the number density distribution of the snow particles by the average amount of charge per snow particle. For simplicity, we assumed that the charge amount of each snow particle was constant. Omiya et al. (2011) measured the charge-to-mass ratios of snow particles at different temperatures and particle sizes in the wind tunnel experiment and estimated that the electric charge per snow particle was $-2 \times 10^{-14}$ C under the conditions of air temperature at −10 C and a particle size of 0.3 mm. The median charge per snow particle at Byrd Station was $-5 \times 10^{-14}$ C when the wind velocity at the height of 50 cm was between 4.5 and 6.5 m/s (Wishart, 1968).

Fifty-seven percent of the wind direction was north-northeast, northeast, and east-northeast at Syowa Station (Sato and Hirasawa, 2007). Northeast wind prevailed during blizzards. When maximum wind speed was observed, the wind directions were north-northeast, northeast, and east-northeast in 29 out of the 30 blizzards identified in 2015 at Syowa Station (Yamamoto et al., 2015; Oshiki, 2016). The ocean extends to the northeast of Syowa Station. The sea surface was frozen during the period of analysis in this paper (Ushio, 2015; Miura, 2016). During the blizzard, many snow particles were negatively charged because they migrated into Syowa Station with repeated saltations at the snow surface on the sea ice. The charge amount of the snow particles depends on the transported length with snow surface collisions (Omiya and Sato, 2011). This implies that the charge accumulated with multi-collisions. Therefore, we considered the possibility that the charge amount in the calculation would be larger and smaller than that in previous studies (Wishart, 1968; Omiya and Sato, 2011). The charge amounts were given by $-1 \times 10^{-13}$, $-1 \times 10^{-14}$, and $-1 \times 10^{-15}$ C per snow particle.

We used the density distribution of snow particles observed at Halley Station, Antarctica, obtained by Mann et al. (2000). They measured the snow-particle number flux and presented the 10-minute mean profile of snow particle number density into eight wind speed bins ranging between 10 and 17 m/s (1.0 m/s bin width). These profiles showed that the number density of snow particles decreased with height following a power law. We formulated the number of snow particles per unit volume, $n_w$(z), as a function of height, $z$, for each wind velocity bin $w$, as depicted in Mann et al. (2000), with the constant values $a_w$ and $b_w$ shown as follows:

$$n_w(z) = 10^{\,kw(z)}, \text{ where } k_w(z) = a_w\, z + b_w. \qquad (5)$$

For $w$ = 15–16 m/s, we derived the coefficients of $a_w = -0.67$ and $b_w = 6.37$. Fig. 10 shows the height distribution of the number of snow particles per $10^{-6}$ m$^3$ (1 cm$^3$).

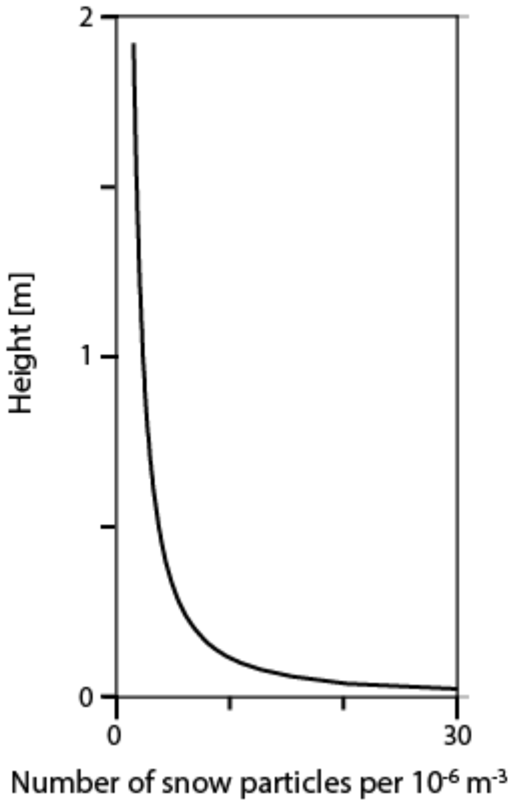


Fig. 10. Height distribution of the number density of snow particles depicted in Mann et al. (2000) for the Poisson calculation. The horizontal and vertical axes denote the number of snow particles per $10^{-6}$ m$^3$ and the height (i.e., $z$), respectively.

The sensor of the electric field mill was installed at 1.4 m in height and mounted downward using a metal pipe (Fig. 1). The measured value of the grounding resistance of the sensor was 100 Ω. Assuming that the constant permittivity and conductivity of the snow surface are $\varepsilon$ and $\kappa$, the relaxation time $T_{relax}$ is represented by the following equation (Harrison et al., 2016):

$$T_{relax} = \varepsilon/\kappa. \qquad (6).$$

Gow (1968) sampled snow and ice on the surfaces and in the boreholes at several sites in Antarctica and Greenland and measured their electric conductivity. The conductivity of the snow and ice was 1 to 2 × $10^{-4}$ S/m at inland sites. The conductivity at Little America V (78°11'S, 162°12'W), located on the Ross Ice Shelf near the sea, was about 6 × $10^{-4}$ S/m. The relative permittivity measured at a depth of 1 m in Antarctica was between 1.4 and 2.0 (Sugiyama et al., 2010). Since the permittivity of the air was 8.9 × $10^{-12}$ F/m when the conductivity was assumed to be $10^{-4}$, the relaxation time was about $10^{-7}$ seconds, which was negligible. The sensor unit of the electric field mill and the metal pipe mounting the sensor unit (Fig. 9) were grounded. The three-dimensional Poisson calculations were carried out with the above charge and conductor distribution as initial and boundary conditions.

Fig. 11 shows the electric field distribution on the plane (red plane in Fig. 9a) across the sensor unit of the electric field mill. The electric field in fair weather without and with the sensor unit is shown in Fig. 11a and b, respectively. Fig. 11c shows the electric field with the sensor unit in the distribution of snow particles (i.e., during the blizzard), based on the observation of Mann et al. (2000). The electric charge was −1 × $10^{-14}$ C per snow particle.

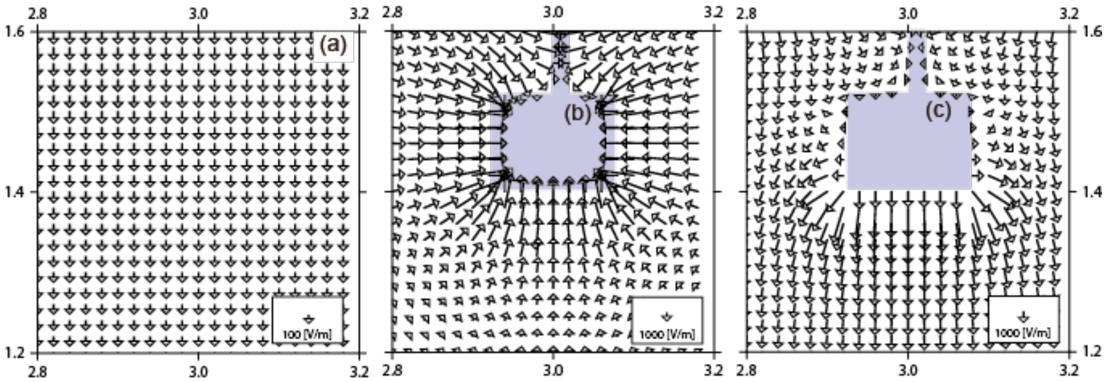


Fig. 11. Electric field in the three-dimensional Poisson calculation. A cross-section (red plane in Fig. 9a) across the sensor unit is shown. The arrows indicate the direction and magnitude of the electric field. The area of the conductor corresponding to the sensor unit and metal pipe is shaded. The calculation results are as follows: (a) in fair-weather without the sensor unit, (b) in fair-weather with the sensor unit, and (c) during the blizzard with the electric charge amount of -1 × $10^{-14}$ C per snow particle, with the sensor unit.

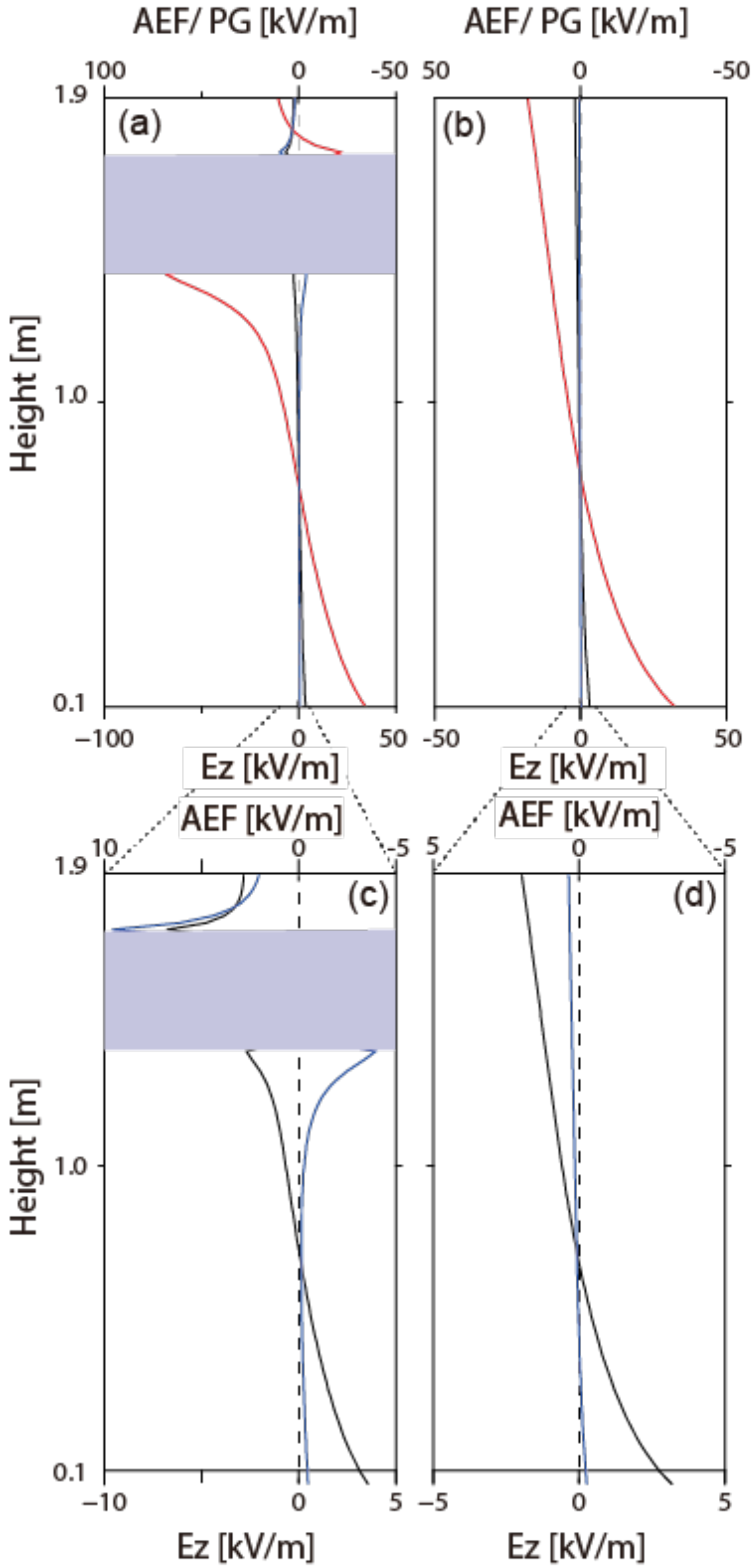


Fig. 12. Vertical distribution of the *z*-component of the electric field in the three-dimensional Poisson calculation. The number density of snow particles during the blizzard as an initial condition was based on Mann et al. (2000). The red, black, and blue lines indicate the calculation results for the charge amounts of $-1 \times 10^{-13}$, $-1 \times 10^{-14}$, and $-1 \times 10^{-15}$ C per snow particle,

respectively. (a), (b) The $z$-component of the electric field along a vertical line (red line in Fig. 9b) through the sensor unit. There is a conductor of the sensor unit from 1.4 m to 1.7 m in height. (c), (d) The $z$-component of the electric field along a vertical line (blue line in Fig. 9b), not passing through the sensor unit. The wide and narrow ranges of the AEF/PG are shown in (a), (c), and (b), (d), respectively.

When the direction of the electric field is from outside to inside the sensor electrode of the electric field mill, it is positive. In other words, the arrows heading to the field mill at the undersurface of the sensor indicate a fair-weather electric field. Fig. 11b shows the calculated electric field reproducing the positive electric field in fair weather. Conversely, the electric field heading away from the sensor electrode was measured as a negative electric field. The result of the calculation shown in Fig. 11c during the blizzard did not provide the electric field heading away to the sensor unit. From this result, the negative electric field was expected to be measured by the calculation but not observed in the field. Therefore, the intense positive electric field observed during the blizzard, shown in Figs. 4 and 6, was not reproduced.

Fig. 12 shows the distribution of the electric field on the $z$-axis during the blizzard. The $z$ component of the calculated electric field on the vertical line passing through the sensor unit (red line in Fig. 9b) and on the line not passing through the sensor unit (blue line in Fig. 9b) are shown in Fig. 12a and 12b, respectively. The calculation results with electric charge amounts of $-1 \times 10^{-13}$, $-1 \times 10^{-14}$, and $-1 \times 10^{-15}$ C per snow particle are shown as red, black, and blue lines, respectively. The electric field of the $z$-component was negative, and this corresponds to arrows heading away at the undersurface of the sensor just below the electric probe of the sensor unit in Fig. 11. In this case, the output value of the electric field mill was negative. The magnitude of the electric field varied widely depending on the charge amount of the snow particles.

The electric field showed a downward direction just below the electric probe of the sensor unit, corresponding to the electric field from the inside to the outside of the sensor unit, as shown in Fig. 11. In this case, the output value measured by the electric field mill was negative. The magnitude of the electric field varied widely depending on the charge amount of the snow particles.

## 4. Discussion

The observed AEF/PG values and calculated electric field values during blizzards were different. The installation method for the electric field mill is described in Section 6.1.2 of MacGorman and Rust (1998). They mentioned that the electric probe of the sensor unit facing downward into the ground (inverted sensor) effectively avoided the electrical noise caused by the charged particles attached to the sensor when charged particle precipitation, such as rain and snow, was falling. Ogawa (1973) estimated that the electric field caused by rain precipitation was 1 kV/m, based on the measurement of the electric current generated by raindrops reported by Ogawa (1960). From the estimation, the polarity of the electric field was opposite to that of the charge of the raindrops. Moreover, the inverted sensor in the condition of the blizzard was ineffective at avoiding the charged snow particles attaching to the sensor because the suspended and saltating snow particles were reachable, even to the inverted sensor. Thus, we concluded that the positive intense AEF/PG values observed during the blizzard were apparent electric field measurements because of collisions of charged snow particles with the sensor electrodes.

After a blizzard, the suspended and saltating snow particles fell onto the snow surface with a negative charge. Although the relaxation time of the charge on the solid snow surface was negligible, as shown in equation (6), the charged snow particles softly attaching to the surface took a certain time to discharge. Sims et al. (2003) calculated the discharge decay-time constant (i.e., the time to reach the charge of $1/e$) for various powders on the surface. The discharge decay times of the Mars dust simulants and acrylic polymer powders were about 5 minutes and 150 minutes, respectively. We carried out the Poisson calculation under the initial condition that a thin layer of negatively charged snow particles was covered on the snow surface (Figs. 13 and 14). The results of the Poisson calculations shown in Fig. 13 indicated that when the negative charge density for the thin layer on the surface was $-1 \times 10^{-8}$ C/m$^2$, an electric field heading away from the field mill sensor was reproduced. Fig. 14 shows that when the negative charge density was $-1 \times 10^{-7}$ C/m$^2$ or $-1 \times 10^{-8}$ C/m$^2$, the calculated electric field was opposite to that of $-1 \times 10^{-9}$ C/m$^2$. Assuming that the distribution of the number density of snow particles followed that of Mann et al. (2000) and that the electric charge per snow particle was $-1 \times 10^{-14}$ C, the charge density layer on the surface became $-5.5 \times 10^{-8}$ C/m$^2$ when the suspended and saltating snow with the negative charge from the ground to 1.0 m fell into the surface.

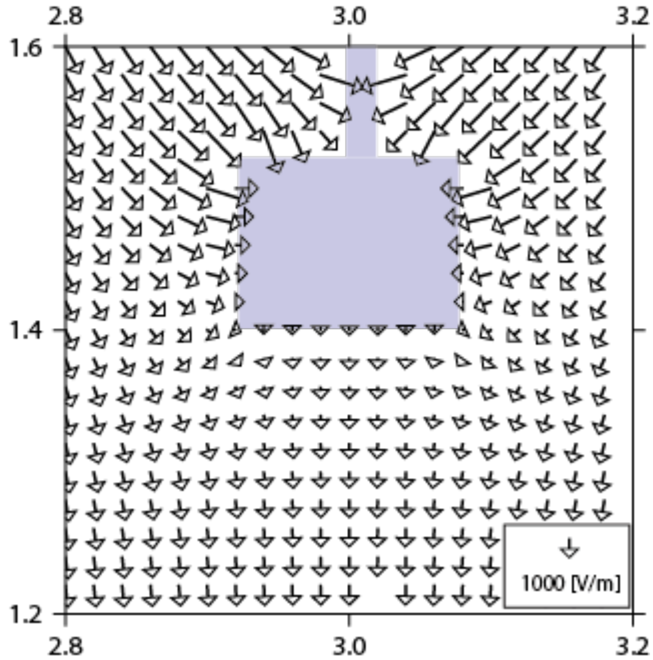


Fig. 13. Electric field with the negatively charged snow-particle layer on the surface of $-1 \times 10^{-8}$ C/m$^2$ on the cross-section (red plane in Fig. 9a) across the sensor unit is shown. The arrows indicate the direction and magnitude of the electric field. The area of the conductor corresponding to the sensor unit and metal pipe is shaded.

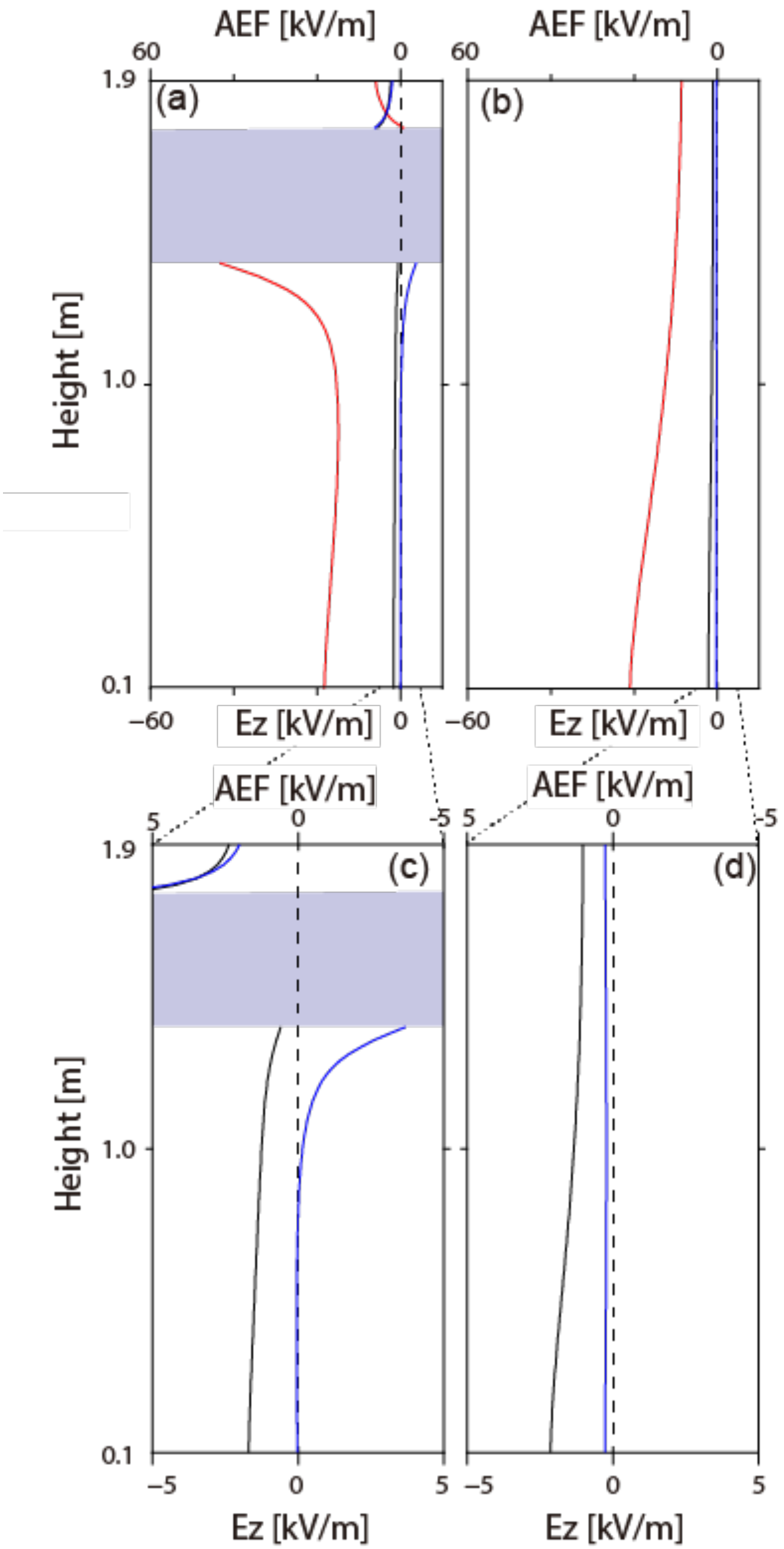


Fig. 14. Vertical distribution of the electric field *z*-component with the initial condition of which the negatively charged snow particle layer on the surface is shown. The red, black, and blue lines indicate the calculation results, in which the charge densities are $-1 \times 10^{-7}$, and $-1 \times 10^{-8}$ C/m$^2$, $-1 \times 10^{-9}$, respectively. (a), (b) The *z*-component of the electric field along a vertical line (red

line in Fig. 9b) through the sensor unit. There is a conductor of the sensor unit from 1.4 m to 1.7 m in height. (c), (d) The *z*-component of the electric field along a vertical line (blue line in Fig. 9b), not passing through the sensor unit. The wide and narrow ranges of the AEF/PG are shown in (a), (c), and (b), (d), respectively.

The live camera was located more than 100 m away from the sensor unit of the electric field mill. The height of the camera (30 m) was higher than that of the electric field mill sensor (1.4 m). Therefore, it was difficult for the still images recorded by the camera to verify the presence of powdered snow on the ground because of insufficient image resolution. The LPM sensor for measuring the NPP, shown in Figs. 4 and 6, was mounted at a height of 4.4 m, and the snow particle layer was not measured. However, the origin of the negative electric field just after the blizzard was explained, assuming that the presence of the snow-particle layer originated from the falling of suspended and saltating snow particles to the ground.

We found a correlation between the duration of the negative AEF/PG and the magnitude of the electric field: The larger the magnitude of the negative electric field value was, the longer the duration of the negative AEF/PG value became. This correlation was understandable when we speculated about the relationship between the time required for the discharge of the snow particles softly attaching to the snow surface and the amount of electric charge of the snow particles. However, monitoring the distribution of snow particles and the electric charge of the particles just above the ground surface may enable us to verify this speculation, as it remains a problem for future consideration.

Although the electric field mill is generally used for the observation of AEF/PG, the measurements do not reflect the signal originating from the charged particle distribution, particularly under severe conditions, such as in desert and polar regions. Nicoll et al. (2020) observed a positive AEF/PG exceeding 7 kV/m, generated by charged desert dust at Al Ain in the United Arab Emirates. Renno et al. (2008) developed an electric field mill for Mars. They mentioned that a typical dust storm on Mars, such as with a charge density of $10^{-8}$ C/m$^3$ and a wind velocity of 20 m/s, generates an electric field of about 11 kV/m. Therefore, to monitor the AEF/PG in a dusty environment, signals caused by the collisions of charged particles must be discriminated from the signal of ambient AEF/PG. Furthermore, the measurements of the electric field mill are applicable to automatic storm monitoring because the magnitude of the measured noise is possibly correlated to that of the storm. For instance, the start and end times of blizzards, such as the events at Syowa Station, have generally been identified from ocular observation. However, the electrical observation using the field mill offers unmanned monitoring because the intense positive electric field may be related to visibility. In further application, observations with the field mill were also useful for snow drifting studies in areas with high mountains, such as the Alps and Mt. Fuji, to mitigate snow avalanches (Gauer, 2001) and turbulent electrification monitoring for industrial dust to avoid explosions.

## 5. Conclusion

We investigated the origin of the intense positive AEF/PG during blizzards/snowstorms and the moderate negative AEF/PG just after a blizzard at Syowa Station, Antarctica. A Poisson calculation with the negatively charged snow particles surrounding the sensor unit did not reproduce the observed intense positive AEF/PG during the blizzard. This implies that the intense positive PG during the blizzard should be the apparent electric field variation originating from the suspended and saltating snow particles attached to the sensor. The moderate negative AEF/PG just after the blizzard was reported for the first time. When a moderate negative electric field was observed, the number of snow particles dropped at a point higher than the sensor unit of the electric field mill. We modeled that the charge of the snow particles that had fallen and softly attached to the ground on the ground surface remained during the negative AEF/PG. The Poisson calculation in the model reproduced the negative electric field. Thus, we showed that the origins of the intense positive and moderate negative electric fields during and after blizzards are the charged snow particles colliding with the electric probe on the sensor unit and the negative snow layers softly attached to the ground.

## Acknowledgments

The authors thank Y. Kimura, Y. Suzuki, and T. Ishikawa (Tokyo Gakugei University) for their help and discussion. The Japan Meteorological Agency (JMA) provides 1-minute wind velocity data. The AEF data are provided by the University of Shizuoka and the National Institute of Polar Research (NIPR), Japan. The data on the NPPs and time-lapse images are provided by the National Institute of Polar Research (NIPR). Fig. 1 was created using the map "Syowa Station" at a scale of 1:2,500 by the Geographical Survey Institute of Japan. This study was part of the Science Program (AP41 and AP905) of the Japanese Antarctic Research Expedition (JARE; YM, MK, AK, and SM). It was supported by NIPR under MEXT and NIPR through General Collaboration Project No. 23-12 (YM, MK, and AK), 26-13 (YM, MK, AK, and SM), and 29-15 (YM, MK, AK, and SM). The authors are grateful to the JARE members for their efforts to maintain the AEF and other observation equipment at Syowa Station. This research was also supported in part by the Joint Support-Center for Data Science Research ROIS-DS-JOINT 2018 and 2020 (YM, MK, AK, and SM), research project no. 2019-01 (YM, MK, AK, and SM), Institute of Oceanic Research and Development, Tokai University (MK), and JSPS KAKENHI Grant Number 20H02419 (MK).

## References

Aplin, K.L., 2018. Atmospheric electricity at Durham: the scientific contributions and legacy of JA ("Skip") Chalmers (1904–1967). Hist. Geo Space. Sci. 9(1), 25–35.

Anderson, R.S., 1987. Eolian sediment transport as a stochastic process: the effects of a fluctuating wind on particle trajectories. J. Geol. 95, 497–512.

Asuma, Y., Kikuchi, K., Taniguchi, T., Fujii, S., 1988. Vertical structures of the atmospheric electrical potential gradient and the behavior of the precipitation charges during snowfalls near the ground surface. J. Meteorol. Soc. Jpn. Ser. II. 66, 473–488.

Burrows, D.A., Hobbs, P.V., 1970. Electrical charges on snow particles. J. Geophys. Res. 75, 4499–4505.

Gauer, P., 2001. Numerical modeling of blowing and drifting snow in Alpine terrain. J. Glaciol. 47, 97–110.

Gordon, M., Taylor, P.A., 2009. Measurements of blowing snow, part I: particle shape, size distribution, velocity, and number flux at Churchill, Manitoba, Canada. Cold Reg. Sci. Technol. 55, 63–74.

Gow, A.J., 1968. Electrolytic conductivity of snow and glacier ice from Antarctica and Greenland. J. Geophys. Res. 73, 3643–3649.

Harrison, R.G., 2004. The global atmospheric electrical circuit and climate. Surv. Geophys. 25, 441–484.

Harrison, R.G., 2013. The carnegie curve. Surv. Geophys. 34, 209−232.

Harrison, R.G., Barth, E., Esposito, F., Merrison, J., Montmessin, F., Borlina, C., Berthelier, J.J., Deprez, G., Farrell, W.M., Houghton, I.M.P., Renno, N.O., Nicoll, K.A., Tripathi, S.N., Zimmerman, M., 2016. Applications of electrified dust and dust devil electrodynamics to Martian atmospheric electricity. Space Sci. Rev. 203, 299–345.

Hirasawa, N., Konishi, H., Nishimura, K., Genthon C., 2018. Project group of Japan Meteorological Agency, SPICE site report: Rikubetsu, Japan. WMO Solid Precipitation Intercomparison Experiment SPICE 2012–2015. Instruments and Observing Methods, Report No. 131.

Kikuchi, K., 1970. Observations of the AEF at Syowa Station, Antarctica. J. Meteorol. Soc. Jpn. Ser. II. 48, 452–460.

Latham, J., Montagne, J., 1970. The possible importance of electrical forces in the development of snow cornices. J. Glaciol. 9, 375–384.

Liu, C., Williams, E.R., Zipser, E.J., Burns, G., 2010. Diurnal variations of global thunderstorms and electrified shower clouds and their contribution to the global electrical circuit. J. Atmos. Sci., 67, 309–323.

MacGorman, D.R, Rust, W.D., 1998. The Electrical Nature of Storms. Oxford University Press, London.

Maeno, N., Naruse, R., Nishimura, K., Takei, I., Ebinuma, T., Kobayashi, S., Nishimura H., Kaneda Y., Ishida, T., 1985. Wind-tunnel experiments on blowing snow. Ann. Glaciol. 6, 63–67.

Mann, G.W., Anderson, P.S., Mobbs, S.D., 2000. Profile measurements of blowing snow at Halley, Antarctica. J. Geophys. Res. Atmos. 105, 24491–24508.

Markson, R., 2007. The global circuit intensity: its measurement and variation over the last 50 years. Bull. Amer. Meteor. 88, 223–241.

Minamoto, Y., Kadokura, A., 2011. Extracting fair-weather data from atmospheric electric-field observations at Syowa Station, Antarctica. Polar Sci. 5, 313–318.

Miura, H., 2016. Conditions of weather and sea ice, JARE-56 Report. The 56th Japanese Antarctic Research Expedition Eds. 136–137. (in Japanese).

Nemoto, M., Nishimura, K., 2004. Numerical simulation of snow saltation and suspension in a turbulent boundary layer. J. Geophys. Res. Atmos. 109, D18206.

Nicoll, K.A., Harrison, R.G., Barta, V., Bor, J., Brugge, R., Chillingarian, A., Chum, J., Georgoulias, A.K., Guha, A., Kourtidis, K., Kubicki, M., Mareev, E., Matthews, J., Mkrtchyan, H., Odzimek, A., Raulin, J.-P., Robert, D., Silva, H.G., Tacza, J., Yair, Y., Yaniv, R., 2019. A global atmospheric electricity monitoring network for climate and geophysical research. J. Atmos. Sol.-Terr. Phys. 184, 18-29.

Nicoll, K., Harrison, G., Marlton, G., Airey, M., 2020. Consistent dust electrification from Arabian Gulf sea breezes. Environ. Res. Lett., 15, 084050.

Ogawa, T., 1960. Electricity in rain. J. Geomag. Geoelec. 121, 21–31.

Ogawa, T., 1973. Analyses of measurement techniques of electric field and currents in the atmosphere. Contrib. Geophys. Inst., Kyoto Univ. 13, 111–137.

Omiya, S., Sato A., 2011. Wind tunnel experiment of an electrostatic charge of blowing-snow particles focusing on collision frequency to the snow surface. Seppyo. 73, 205–212. (in Japanese with English abstract).

Omiya, S., Sato, A., Kosugi, K., Mochizuki, S., 2011. Estimation of the electrostatic charge of individual blowing-snow particles by wind tunnel experiment. Ann. Glaciol. 52, 148–152.

Oshiki, N., 2016. Weather analyses, JARE-56 Report. The 56th Japanese Antarctic Research Expedition Eds. 252–255. (in Japanese).

Renno, N.O., Kok, J.F., Kirkham, H., Rogacki, S., 2008. A miniature sensor for electrical field measurements in dusty planetary atmospheres. J. Phys. Conf. Ser. 142, 012075.

Sato, K., Hirasawa, N., 2007. Statistics of Antarctic surface meteorology based on hourly data in 1957–2007 at Syowa Station. Polar Sci. 1, 1–15.

Schmidt, D.S., Dent, J.D., 1993. A theoretical prediction of the effects of electrostatic forces on saltating snow particles. Ann. Glaciol. 18, 234–238.

Schmidt, D.S., Schmidt, R.A., Dent, J.D., 1999. Electrostatic force in blowing snow. Bound-lay Meteorol. 93, 29–45.

Shumilov, O.I., Kasatkina, E.A., Kulichkov, S.N., Kallistratova, M.A., Vasil'ev, A.N., 2005. Meteorological effects in the atmospheric electric field in the high latitudes. Izvestiya Atmos.

Oceanic Phys. 41, 555–562.

Sims, R.A., Biris, A.S., Wilson, J.D., Yurteri, C.U., Mazumder, M.K., Calle, C.I., Buhler, C.R., 2003. Development of a transparent self-cleaning dust shield for solar panels. Proc. ESA-IEEE Joint Meeting on Electrostatics. 814–821.

Sugiyama, S., Enomoto, H., Fujita, S., Fukui, K., Nakazawa, F., Holmlund, P., 2010. Dielectric permittivity of snow measured along the route traversed in the Japanese–Swedish Antarctic Expedition 2007/08. Ann. Glaciol. 51, 9–15.

Suzuki, T., Matsudo, Y., Asano, T., Hayakawa, M., Michimoto, K., 2011. Meteorological and electrical aspects of several winter thunderstorms with sprites in the Hokuriku area of Japan. J. Geophys. Res. Atmos. 116, D06205.

Tsurudome, C., Flaquiere, A., Mochizuki, K., Teuff, Y., Sakai, R., Tuffenis, J., Suzuki, Y., Cohen, D., Fujiwara, H., Inazaki, K., Yahi, S., Nakamura, M., Kamogawa, M. (2013). Measurement of the atmospheric electric field inside the nonthunderstorm clouds on 2012 BEXUS campaign. J. Atmos. Electr. 33, 77−80.

Ushio S., 2015. Conditions of weather and sea ice, JARE-55 Report. The 55th Japanese Antarctic Research Expedition Eds. 147–148. (in Japanese).

Williams, E., Mareev, E., 2014. Recent progress on the global electrical circuit. Atmos. Res. 135, 208–227.

Wishart, E.R., 1968. Electrification of Antarctic drifting snow. Proc. Int. Symp. Antarctic Glaciological Exploration, Hanover 86, 316–324.

World Meteorological Organization, 1966. International Meteorological Vocabulary. Secretariat of the World Meteorological Organization.

Yamamoto, H., Imaizumi, K., Asahara, N., Ohtake, J., Saeki, Y., 2015. Weather, JARE-55 Report. The 55th Japanese Antarctic Research Expedition Eds. 225–242. (in Japanese).

Zheng, X., He, L., Zhou, Y., 2004. Theoretical model of the electric field produced by charged particles in windblown sand flux. J. Geophys. Res. Atmos. 109, D15208.